

Highly Selective Transformation of Biomass Derivatives to Valuable Chemicals by Single-Atom Photocatalyst Ni/TiO₂

Lunqiao Xiong, Haifeng Qi, Shengxin Zhang, Leilei Zhang, Xiaoyan Liu, Aiqin Wang,* and Junwang Tang*

Selective C–C cleavage of the biomass derivative glycerol under mild conditions is recognized as a promising yet challenging synthesis route to produce value-added chemicals. Here, a highly selective catalyst for the transformation of glycerol to the high-value product glycolaldehyde is presented, which is composed of nickel single atoms confined to the surface of titanium dioxide. Driven by light, the catalyst operates under ambient conditions using air as a green oxidant. The optimized catalyst shows a selectivity of over 60% to glycolaldehyde, resulting in 1058 $\mu\text{mol g}_{\text{Cat}}^{-1} \text{h}^{-1}$ production rate, and ≈ 3 times higher turnover number than NiO_x-nanoparticle-decorated TiO₂ photocatalyst. Diverse operando and in situ spectroscopies unveil the unique function of the Ni single atom, which can significantly promote oxygen adsorption, work as an electron sink, and accelerate the production of superoxide radicals, thereby improving the selectivity toward glycolaldehyde over other by-products.

acetic acid, and ketone derivatives.^[1] These chemicals have wide applications as essential molecular building blocks and intermediates for the manufacture of perfumes, dyestuffs, and pharmaceuticals. Because the C–C bond cleavage is thermodynamically unfavorable due to the relatively high C–C bond energy (90 kcal mol⁻¹), the traditional C–C bond cleavage processes, most of which are thermocatalytic reactions driven by energy- and cost-intensive systems, heavily depend upon toxic/expensive oxidants, noble metal catalysts, and often require harsh conditions.^[2] Selective C–C bond cleavage under mild conditions is therefore much sought after as a valuable tool to upgrade biomass-derived polyols.

Glycerol is such a highly versatile polyol and also an important by-product

in biodiesel production which is produced in large quantities, resulting in a huge surplus flooding the market at a very low price (US \$0.11 per kg).^[3] Thus glycerol is regarded as a bio-waste but also one of the top ten biomass-derived platform molecules for the production of high-value chemicals (listed by the U.S. Department of Energy).^[4] Under appropriate conditions, glycerol could be selectively oxidized or reduced into fine chemicals such as acrolein,^[5] dihydroxyacetone,^[6] lactic acid,^[7] acrylic acid,^[8] 1,2-propanediol,^[9] or 1,3-propanediol.^[10] With this potential, substantial efforts have been devoted to exploring an efficient catalyst to achieve high conversion and high selectivity to the targeted products. The gold-on-carbon catalyst is one of the early examples, which is only effective with the presence of NaOH. Therefore, the oxidation products are normally sodium salts, making the post-purification process very difficult.^[11] Thereafter, efforts were devoted to searching for alternative catalysts working without NaOH. More recently, it has been reported that Mn₂O₃ could convert glycerol into glycolic acid with a selectivity of 52.6% at 140 °C and in 1 MPa O₂.^[12] However, it remains a significant challenge to develop efficient, highly selective catalysts for the transformation of glycerol into a specific product. Therefore, selective glycerol C–C cleavage is not only of great scientific significance, but also of economic interest considering the high price of the interested product (e.g., US \$9 per kg of glycolaldehyde, ≈ 80 times more valuable than the reactant glycerol).


Photocatalysis has been recognized as a promising strategy in the C–C bond cleavage reactions under very mild conditions.^[13]

1. Introduction

Biomass resources are produced by the photosynthesis of CO₂ and water using solar energy and are widely available in the natural environment. Driven by the sustainable and environmentally sound use of natural resources, transforming biomass and biomass derivatives into value-added products has gained increasing significance. One of the most important strategies is the C–C bond cleavage of biomass-derived polyols for the synthesis of valuable carbonyl compounds such as aldehydes,

L. Xiong, J. Tang
Department of Chemical Engineering
University College London
Torrington Place, London WC1E 7JE, UK
E-mail: junwang.tang@ucl.ac.uk

H. Qi, S. Zhang, L. Zhang, X. Liu, A. Wang
State Key Laboratory of Catalysis
Dalian Institute of Chemical Physics
Chinese Academy of Sciences
Dalian 116023, P. R. China
E-mail: aqwang@dicp.ac.cn

 The ORCID identification number(s) for the author(s) of this article can be found under <https://doi.org/10.1002/adma.202209646>.

© 2023 The Authors. Advanced Materials published by Wiley-VCH GmbH. This is an open access article under the terms of the Creative Commons Attribution License, which permits use, distribution and reproduction in any medium, provided the original work is properly cited.

DOI: 10.1002/adma.202209646

In contrast to thermal catalytic C–C bond fission processes, it utilizes light as an inexpensive, renewable, and inherently safe energy source to replace harsh conditions.^[14] Several pioneering and insightful works have been dedicated to this area. For example, TiO₂ photocatalysts with different dominant facets were used to selectively convert glycerol to glycolaldehyde in an aqueous solution and inert atmosphere. The product distribution was proved to be dependent on the facets of TiO₂^[14b] while the production rate was rather moderate (e.g., 83.8 μmol g⁻¹ h⁻¹ of glycolaldehyde). Later, a mechanistic picture at the molecular level of photocatalytic C–C bond cleavage of ethylene glycol was developed by coupling in situ surface study with vibrational-mass spectrometry on rutile (110) surface in an ultrahigh vacuum condition.^[15] The C–C bond cleavage was found to be the only route in ethylene glycol photooxidation under deaerated conditions, resulting in the generation of formaldehyde and hydrogen. The rate-determining step in this process is the desorption of the surface-adsorbed hydrogen, making pristine TiO₂ a poor photocatalyst that only catalyzes the ethylene glycol conversion at very low surface coverages. A recent work introduced oxygen into this process, revealing that the presence of oxygen could readily convert organic products into CO₂ via complete oxidation by oxygen, or into paraformaldehyde by polymerization with water.^[16] With this attractive progress so far, the relatively low selectivity in the presence of O₂ requires the rational design of photocatalysts. One barrier is that most semiconductor-based photocatalysts are either non-selective (particularly with the presence of water and/or oxygen) or ineffective to break down the C–C bond because of poor oxidative activity.^[17] This is because once oxygen and/or water are involved as reactants, various strong reactive oxygen species (ROS) could be generated, unselectively mineralizing organic compounds into CO₂ and water.^[18] Moreover, the oxidants and products often encounter diffusion limitations while accessing or desorbing the active centers, leading to poor interfacial contact that affects the catalytic reactions. More importantly, the role of metal (or metal oxide) nanoparticles that are often used as promoters remains unclear and sometimes controversial due to the involvement of complex factors including diverse particle sizes, exposed facets, and chemical states. Single-atom photocatalysts have provided an ideal platform to address the above challenges benefitting from their uniform geometrical/electronic structure, exotic properties, and maximum atom-utilization efficiency.^[19] For example, according to density functional theory (DFT) simulation, when anchoring Ni single atoms on the anatase TiO₂ surface, new vacant levels are formed near the conduction band minimum.^[20] The photogenerated electrons in the TiO₂ conduction band can be readily transferred to the Ni species, thus achieving effective charge separation. These well-defined active sites may open up the possibility of regulating the generation of ROS, tailoring adsorption/desorption properties, and understanding structure-activity relationships.^[21]

Up to now, highly selective photocatalysts for aerobic C–C cleavage of glycerol to valuable chemicals are so challenging with few studies. In this work, earth-abundant Ni single atoms were precisely anchored on TiO₂ by a novel molten-salt method. The photocatalyst can highly selectively cleave the C–C bond of glycerol in the presence of air at room temperature and under atmospheric pressure. Furthermore, diverse in situ and operando spec-

troscopies clarify Ni single atoms as both the oxygen adsorption sites and the acceptor of photogenerated electrons. This bifunction of Ni single atoms efficiently generates superoxide radicals, resulting in over 60% selectivity toward glycolaldehyde, together with high efficiency and long-term stability.

2. Results and Discussion

The Ni single atoms decorated TiO₂ was synthesized via a modified molten-salt method, in which Ni single atoms were loaded onto the TiO₂ surface in metal salts at an elevated temperature.^[22] Afterward, the mixture was washed with a large amount of water to remove the salt residues, which was confirmed by the XPS results (Figure S1, Supporting Information). Ni single atoms decorated TiO₂ synthesized using the above method is denoted as 0.5Ni/TiO₂-MS (0.5 stands for the weight percentage of loaded Ni species). As a comparison, the same amount of Ni species was loaded on the TiO₂ surface by a typical impregnation method, which is denoted as 0.5Ni/TiO₂-IM.

When using these two photocatalysts and pristine TiO₂ for glycerol oxidation under atmospheric air and 365 nm irradiation, a distinctive difference in the glycolaldehyde yield can be observed (Figure 1a). Pristine TiO₂ shows a glycolaldehyde evolution rate of 529 μmol g⁻¹ h⁻¹, with a small selectivity of 23.9%. It should be noted that the selectivity here is calculated based on the carbon balance instead of the molar amount of produced glycolaldehyde. Since the glycerol to glycolaldehyde is a C3-to-C2 reaction, its theoretical maximum selectivity is 66.7%. The introduction of Ni species by the impregnation method has little impact on the selectivity (23.4%) and even somewhat decreases the glycolaldehyde evolution rate (463 μmol g⁻¹ h⁻¹). When dispersing Ni species over TiO₂ by the novel molten-salt method, the catalyst presents a twofold increase in glycolaldehyde evolution rate (1058 μmol g⁻¹ h⁻¹), resulting in an apparent quantum yield (AQY) of 10.3%, again, two times higher than that achieved on TiO₂ (AQY = 5.2%). More importantly ca. twofold enhancement in selectivity (60.1%) has been achieved on 0.5Ni/TiO₂-MS compared with pristine TiO₂. By comparison, transition metal species, including Ag, Au, and Cu were also loaded on TiO₂ via the impregnation method and molten-salt method. Evaluation of the evolution rate and more importantly the selectivity under identical conditions (Figure S2, Supporting Information) suggests that Ni can represent the highest selectivity of 60.1%, which is close to the maximum theoretical selectivity (66.7%) to glycolaldehyde, nearly doubling the selectivity achieved on noble metal loaded TiO₂.

We thus further investigated the effect of the Ni species loading amount on the catalytic performance. The metal loading was verified by inductively coupled plasma atomic emission spectrometry (ICP-AES) measurements (Table S1, Supporting Information). Both pristine TiO₂ and 0.5Ni/TiO₂-IM tend to unselectively oxidize glycerol into various products, including formic acid, glycolaldehyde, dihydroxyacetone, and glyceraldehyde (Figure 1b), consistent with the previous reports.^[14b] Among them, formic acid accounts for the largest yield, indicating the unselective nature to high-value chemicals. When using 0.5Ni/TiO₂-MS, the yield toward glycolaldehyde is greatly enhanced. More importantly, the selectivity to glycolaldehyde

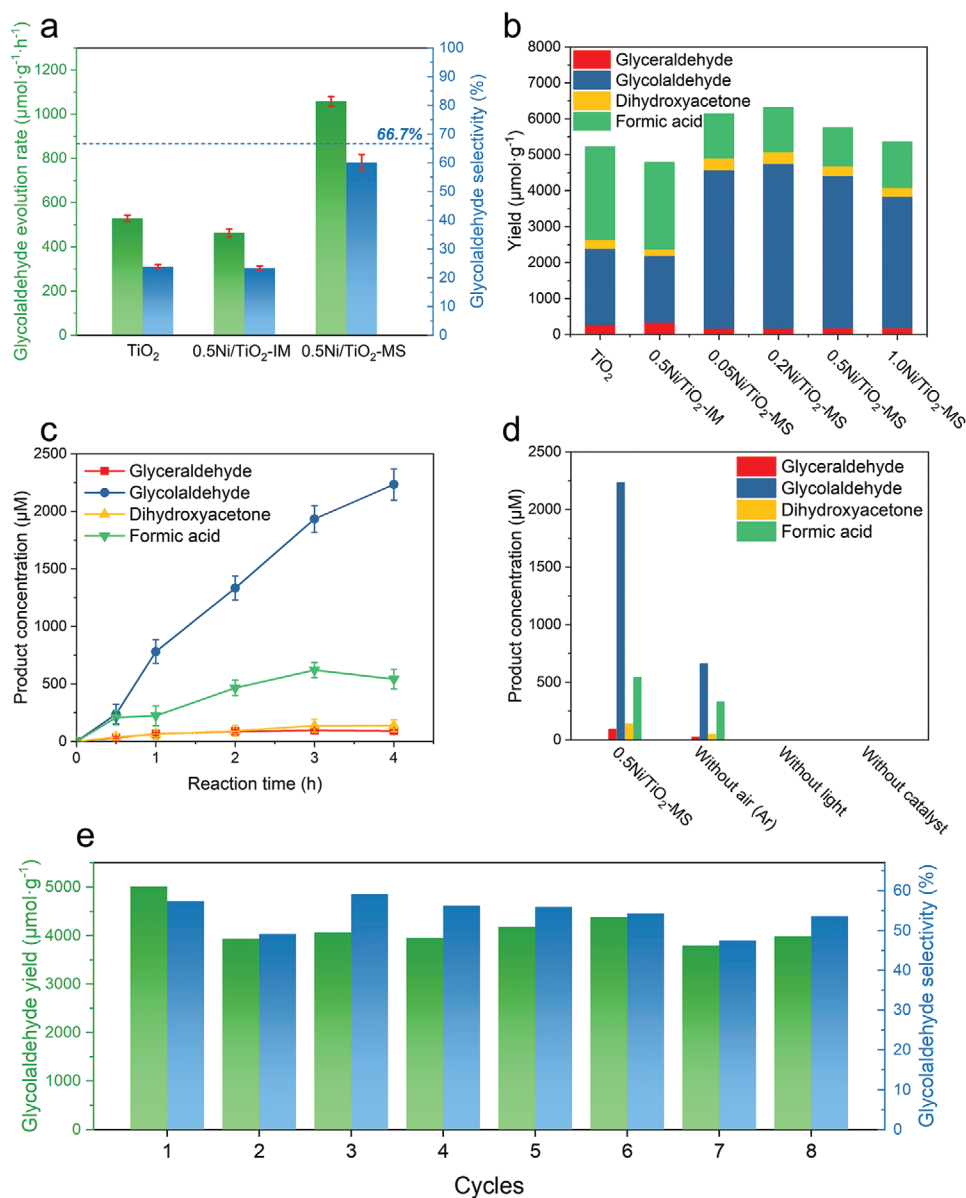


Figure 1. a) The evolution rate and selectivity of glycolaldehyde over TiO_2 , 0.5Ni/ TiO_2 -IM, and 0.5Ni/ TiO_2 -MS. b) The product distribution over different catalysts. c) The temporal synthesis of different products over 0.5Ni/ TiO_2 -MS. d) Product yields from a series of control experiments. e) Stability test of 0.5Ni/ TiO_2 -MS for eight cycles reaction. Reaction conditions: 15 mg catalyst, 30 mL of 25 mM glycerol aqueous solution, 25 °C, air at atmospheric pressure, 365 nm light irradiation, 4 h reaction time if denoted otherwise.

increases with the Ni loading amount until 0.5%, such as from 38.6% on 0.05Ni/ TiO_2 -MS to 60.1% on 0.5Ni/ TiO_2 -MS. These results indicate that the Ni species loaded by the molten-salt approach plays an important role in oxidative C–C bond cleavage of glycerol. Further increasing the loading amount to 1.0% leads to a decreased selectivity to glycolaldehyde (39.1%), which could be owing to the new states formed above the TiO_2 valence band. This shifts the oxidation potential of the composite system to a higher position compared to the bare surface, weakening the oxidation power of the holes, and thus decreasing the activity.^[20]

The temporal production of different products over 0.5Ni/ TiO_2 -MS was then monitored to understand the oxidation

process (Figure 1c). Dihydroxyacetone and glyceraldehyde, two C3 products, remain at a low concentration during the whole process, likely due to the consecutive conversion to C2 products and formic acid. (Figure S3, Supporting Information).^[1b] The yield ratio of glycolaldehyde and formic acid is 1:1 after 0.5 h reaction. However, the subsequent increase of formic acid becomes very slow while glycolaldehyde production keeps its momentum, likely due to the further oxidation of formic acid into CO_2 (Table S2, Supporting Information). Pristine TiO_2 and 0.5Ni/ TiO_2 -IM almost show identical product distribution when oxidizing glycerol: generating formic acid and glycolaldehyde at a similar rate (Figure S4, Supporting Information). Considering the oxidation of formic acid into CO_2 is

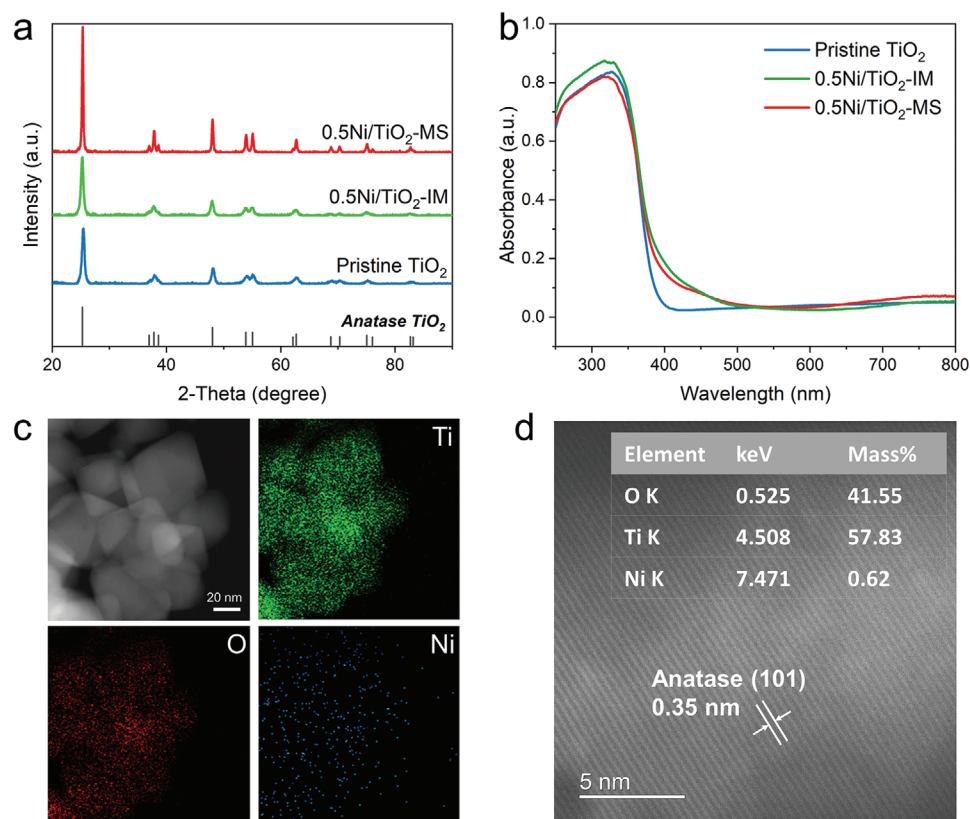


Figure 2. a) XRD patterns and b) UV-vis spectra of TiO_2 , $0.5\text{Ni}/\text{TiO}_2\text{-IM}$, and $0.5\text{Ni}/\text{TiO}_2\text{-MS}$. c) TEM image of $0.5\text{Ni}/\text{TiO}_2\text{-MS}$ and the corresponding EDX elemental mapping. d) HAADF-AC-STEM images of $0.5\text{Ni}/\text{TiO}_2\text{-MS}$ and the corresponding EDX results.

quite fast over the TiO_2 surface,^[1b] a relatively large amount of CO_2 is detected during this process (Table S2, Supporting Information). Meanwhile, glycolaldehyde can also be oxidized to CO_2 on TiO_2 or $0.5\text{Ni}/\text{TiO}_2\text{-IM}$, while the overoxidation of glycolaldehyde is avoided on $0.5\text{Ni}/\text{TiO}_2\text{-MS}$, which induces a large difference in the selectivity. Control experiments were then carried out and the results are presented in Figure 1d. First, without the presence of air, the $0.5\text{Ni}/\text{TiO}_2\text{-MS}$ catalyst shows sharply decreased glycolaldehyde yield, highlighting the importance of oxygen in the air for the reaction. Under dark conditions or without a catalyst, no oxidation products can be detected. Hence, it could be confirmed that all the glycolaldehyde is generated from glycerol photocatalytic oxidation over $0.5\text{Ni}/\text{TiO}_2\text{-MS}$ using air as the oxidant. Figure 1e presents the stability of the best $0.5\text{Ni}/\text{TiO}_2\text{-MS}$ catalyst. The catalyst shows a similar glycolaldehyde yield and selectivity across eight 4 h runs, indicating the excellent stability of the catalyst during the C–C cleavage reaction.

To reveal the mechanism behind the high selectivity to glycolaldehyde over $0.5\text{Ni}/\text{TiO}_2\text{-MS}$, the crystal structure, morphology, and light-harvesting properties of these samples were studied. X-ray diffraction (XRD) patterns of $0.5\text{Ni}/\text{TiO}_2\text{-IM}$ show little difference compared with pristine TiO_2 ; no new peak appears after the impregnation of Ni species due to its low loading amount (Figure 2a). For $0.5\text{Ni}/\text{TiO}_2\text{-MS}$, the sharpened XRD peaks indicate that an enhanced crystallinity of TiO_2 is achieved during the molten-salt treatment. This is because

a higher temperature ($500\text{ }^\circ\text{C}$) was used in the molten-salt method compared with $400\text{ }^\circ\text{C}$ in the impregnation method.^[22] To rule out the effect of crystallinity on the product distribution, $0.5\text{Ni}/\text{TiO}_2\text{-IM}$ was also annealed at $500\text{ }^\circ\text{C}$ under an argon atmosphere for two hours, and no obvious catalytic performance change is observed (Table S3, Supporting Information). Thus, the enhanced selectivity to glycolaldehyde is not because of the improved crystallinity. XRD patterns of molten-salt prepared samples do not present any peaks of metallic or oxide Ni species even increasing the loading amount to 1.0%, indicating that the metal species are highly dispersed over the surface of TiO_2 by this novel method (Figure S5, Supporting Information).

The ultraviolet-visible (UV-vis) spectra (Figure 2b) of the prepared samples present the characteristic absorption band with an onset edge at $\approx 366\text{ nm}$, indicating a bandgap of $\approx 3\text{ eV}$, consistent with the widely reported value (Figure S6a, Supporting Information).^[23] The loading of Ni species by impregnation or molten-salt method has no obvious effect on the onset edge of the samples, besides leading to a slight absorption in the visible-light region (Figure 2b and Figure S6b,c, Supporting Information). This should not affect the photocatalytic activity due to a 365 nm light source being used for excitation. Combining with the XPS valence band spectra (Figure S7, Supporting Information), in which all samples show a similar valence band of 2.7 eV , loading Ni either by impregnation or molten-salt method does not change the band edge positions of photocatalysts.

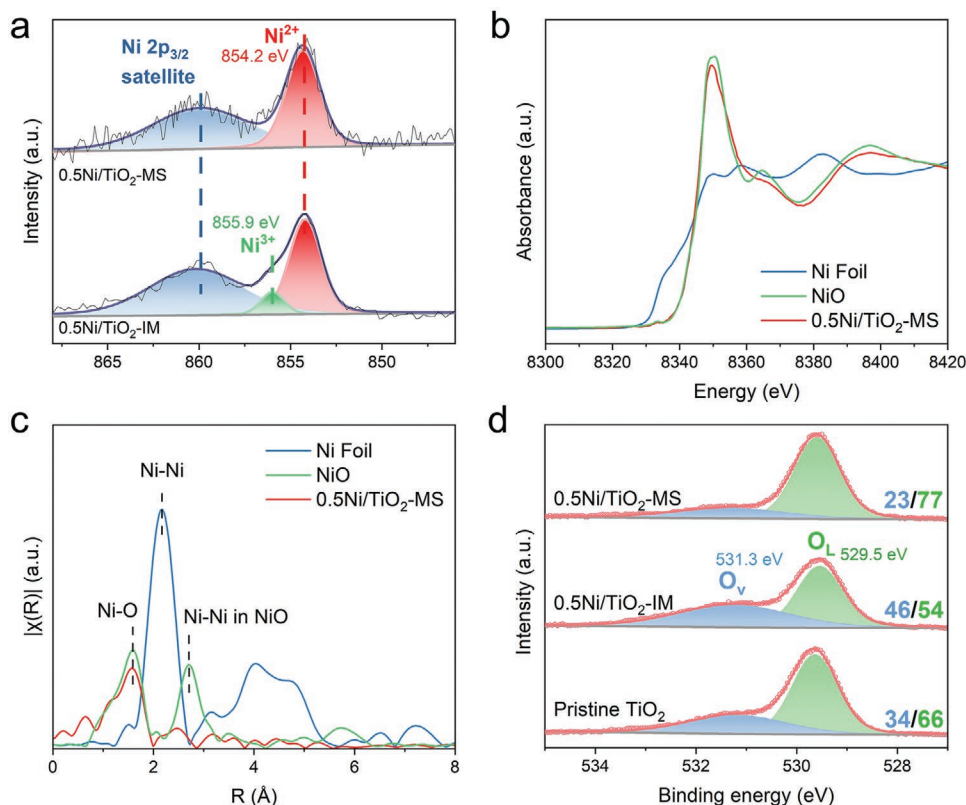


Figure 3. a) Ni 2p_{3/2} XPS spectra of 0.5Ni/TiO₂-IM and 0.5Ni/TiO₂-MS. b) Nickel K-edge XANES results of nickel (metal), NiO 0.5Ni/TiO₂-IM, and 0.5Ni/TiO₂-MS. c) Fitting details for nickel K-edge EXAFS spectra of 0.5Ni/TiO₂-MS. d) O1s XPS results of TiO₂, 0.5Ni/TiO₂-IM, and 0.5Ni/TiO₂-MS.

The morphology of 0.5Ni/TiO₂-MS was first investigated by transmission electron microscopy (TEM), as shown in Figure 2c. The TiO₂ nanoparticles have an average diameter of ≈60 nm. There are no particles on 0.5Ni/TiO₂-MS, while energy-dispersive X-ray (EDX) mapping shows a homogeneous distribution of nickel species. This indicates that Ni species may atomically disperse on the TiO₂ surface. To confirm this hypothesis, we then employed sub-Ångström-resolution high-angle annular dark-field scanning transmission electron microscopy (HAADF-STEM) technique to study the highly dispersed Ni species (Figure 2d), no clusters or nanoparticles can be seen on 0.5Ni/TiO₂-MS sample. Though no bright dots could be distinguished from the STEM image due to the low contrast between Ni and Ti,^[22,24] EDX scanning shows 0.62% of nickel in the scanned area, which is close to the actual amount (0.43%). This strongly suggests the presence of atomically dispersed Ni atoms on the surface of TiO₂ that play an important role during glycerol oxidation (Figure S8, Supporting Information). On the contrary, nanoparticles (likely NiO) with an average diameter of cal. 1.2 nm are formed when using the impregnation method to load Ni species (Figure S9, Supporting Information).

For a deeper understanding of the mechanism behind the high selectivity to glycolaldehyde over 0.5Ni/TiO₂-MS, the chemical states of nickel species were characterized by X-ray photoelectron spectroscopy (XPS) (Figure 3a). The peak located at ≈854 eV is associated with the nickel 2p_{3/2},^[25] and the typical Ni 2p_{3/2} satellite peak is present.^[26] In 0.5Ni/TiO₂-IM, Ni 2p_{3/2} is dominated by the peak at 854.2 eV which corresponds to Ni²⁺,

and there is a minor peak at 855.9 eV which is ascribed to Ni³⁺. The formation of Ni³⁺ on 0.5Ni/TiO₂-IM is likely due to the oxidative environment in the air under 400 °C during the impregnation process. Thus, the nanoparticles on 0.5Ni/TiO₂-IM could be identified as NiO_x (mixed Ni²⁺ and Ni³⁺). For 0.5Ni/TiO₂-MS, the Ni 2p_{3/2} peak indicates that the chemical state of Ni species is mainly +2 (854.2 eV), which is well-maintained even after the 32 h run (Figure S10, Supporting Information).^[27] Therefore, it could be confirmed that different loading methods lead to different Ni species: the novel molten salt method forms Ni²⁺ single atoms while the impregnation method generates NiO_x nanoparticles on the TiO₂ surface.

The chemical state of the nickel species over 0.5Ni/TiO₂-MS was further confirmed by X-ray absorption near-edge structure (XANES) spectroscopies (Figure 3b). The E₀ for 0.5Ni/TiO₂-MS is close to that of NiO, indicating Ni atoms carry positive charges of +2. The coordination environment of Ni single atoms was determined by the extended X-ray absorption fine structure spectra (EXAFS). As shown in the Fourier-transformed k² weighted EXAFS spectra at the Ni K-edge (Figure 3c), unlike the reference samples of Ni foil and NiO, the 0.5Ni/TiO₂-MS catalyst does not show any obvious peaks at the positions of either Ni–Ni shell (2.2 Å) or Ni–O–Ni (2.7 Å) shell, excluding the existence of metallic Ni or NiO_x nanoparticles.^[22] The absence of Ni–Ni scattering was further verified by the wavelet transform technique (Figure S11, Supporting Information). The EXAFS data-fitting results (Table S4, Supporting Information) show that the Ni–O coordination number is 5.2, suggesting

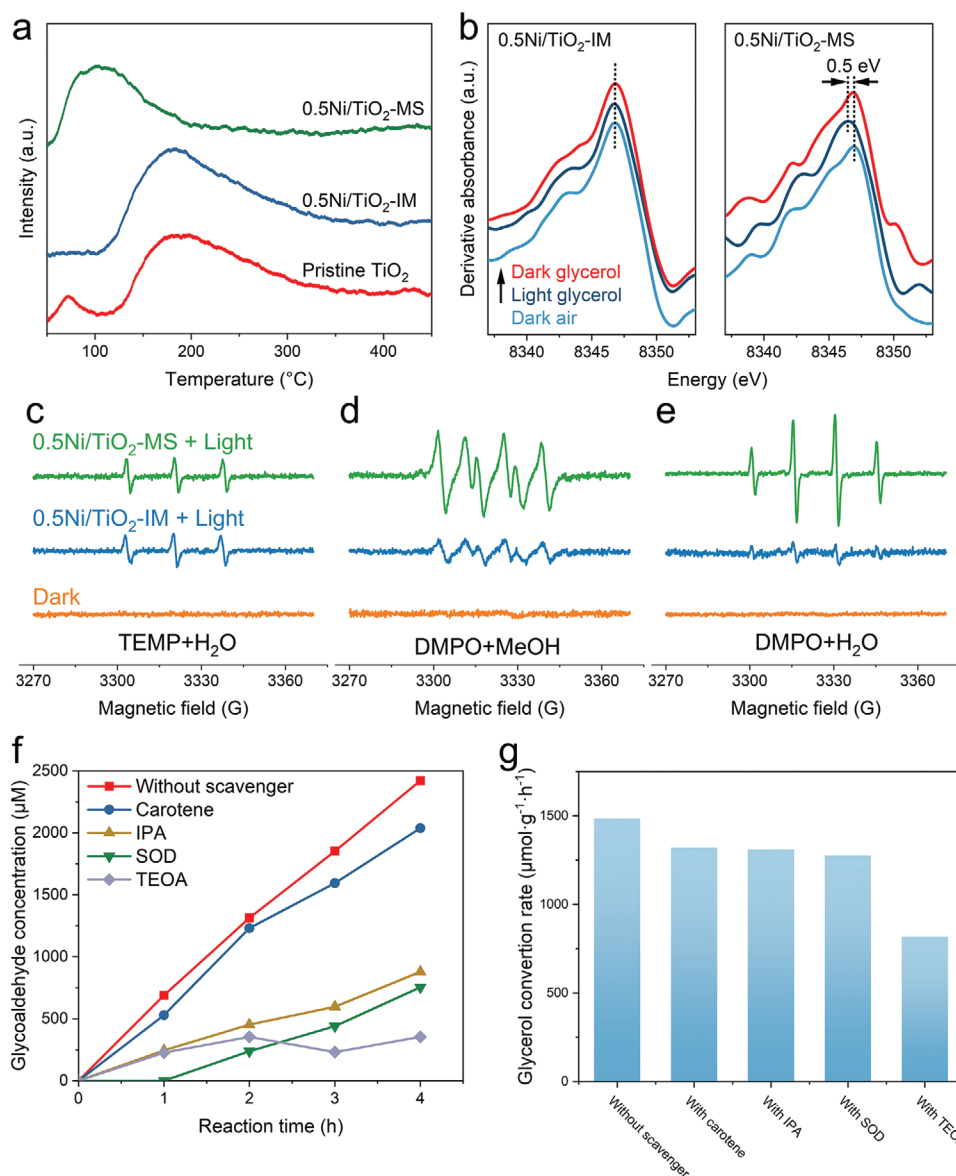


Figure 4. a) O_2 -TPD of TiO_2 , $0.5Ni/TiO_2$ -IM and $0.5Ni/TiO_2$ -MS. b) Derivative data of operando Ni K-edge XANES results of $0.5Ni/TiO_2$ -IM and $0.5Ni/TiO_2$ -MS under different conditions. c) ESR spectra for the detection of 1O_2 on $0.5Ni/TiO_2$ -IM and $0.5Ni/TiO_2$ -MS under air in TEMP aqueous solution. d) ESR spectra under air for the detection of $O_2^{\cdot-}$ on $0.5Ni/TiO_2$ -IM and $0.5Ni/TiO_2$ -MS. e) ESR spectra under air for the detection of $\cdot OH$ on $0.5Ni/TiO_2$ -IM and $0.5Ni/TiO_2$ -MS. f) Glycolaldehyde yield of glycerol oxidation on $0.5Ni/TiO_2$ -MS with different scavengers. g) Effect of different scavengers on the glycerol conversion rate on $0.5Ni/TiO_2$ -IM.

the NiO_5 entities are selectively fabricated. Combining with the XANES data, it could be confirmed that the oxidized state of Ni species is atomically dispersed over TiO_2 , consistent with the HAADF-AC-STEM images.

High-resolution O 1s XPS spectra were also recorded to investigate the surface property of different catalysts (Figure 3d). There are two peaks in the O 1s core level: one peak at 529.5 eV is assigned to the lattice oxygen (O_L) over TiO_2 , while another peak located at 531.3 eV is attributed to oxygen vacancy (O_V).^[28] The O_V/O_L ratio in $0.5Ni/TiO_2$ -IM is 46/54, which is higher than that in pristine TiO_2 (34/66). On the contrary, the $0.5Ni/TiO_2$ -MS sample shows a decreased content of oxygen vacancies (23/77), likely due to the rearrangement of atoms during

molten-salt treatment and consistent with the enhanced crystallinity evidenced by XRD patterns.

Heterogeneous photocatalytic reactions involve three consecutive steps, beginning with the adsorption of the reactants, then the charge generation and transfer, and lastly the surface reaction and product desorption. We next attempted to explore these steps to clarify the function of Ni single atoms. Control experiments prove that oxygen is the major oxidant in glycerol C–C cleavage reaction, it is thus of vital importance to clarify the oxygen adsorption behavior over different catalysts. Figure 4a presents the patterns of temperature-programmed desorption of oxygen (O_2 -TPD) recorded on these samples. Two desorption peaks are observed in pristine TiO_2 : the first one is

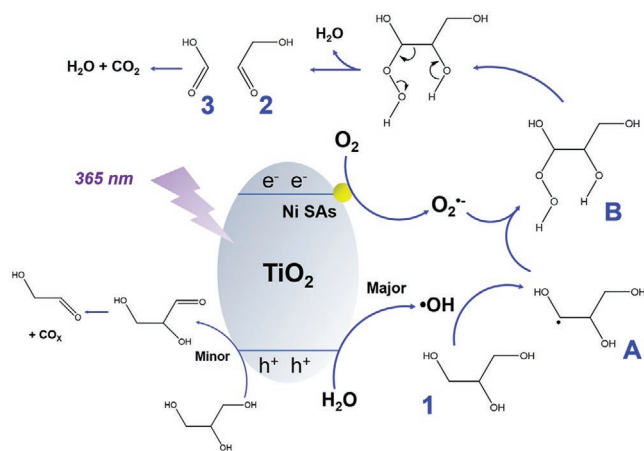
located at 70 °C, which can be assigned to physically-adsorbed O₂, while the second one is ≈150–250 °C, corresponding to chemically-bonded molecular oxygen on O_v.^[29] The O₂-TPD pattern of 0.5Ni/TiO₂-IM presents a similar peak at 150–250 °C with a larger peak area of 1.387 compared with that of pristine TiO₂ (1.154). This trend is consistent with the increased oxygen vacancy amount evidenced by XPS results. As no new peak appears on the 0.5Ni/TiO₂-IM O₂-TPD patterns, it is reasonable to deduce that NiO_x nanoparticles are not able to serve as O₂ adsorption sites, which is consistent with previous reports.^[30] For 0.5Ni/TiO₂-MS, the major desorption peak shifts to a lower temperature (70–200 °C), suggesting the emergence of different oxygen adsorption sites formed on the surface. Considering the decreased oxygen vacancy amount, the only feasible adsorption sites of oxygen on the surface of 0.5Ni/TiO₂-MS are the single Ni atoms.^[31] The left-shifted desorption peak suggests a lower oxygen adsorption energy of single Ni atoms compared with that of oxygen vacancies, such a trend is in agreement with reported values (20 meV for Ni single atoms and 47 meV for oxygen vacancies over TiO₂).^[32]

Following O₂ adsorption, the next vital step for glycerol oxidation is the charge transfer and activation of O₂. The in situ Ti 2p XPS spectra of 0.5Ni/TiO₂-MS indicate that the chemical states of Ti species in the TiO₂ support remain unchanged under UV irradiation (Figure S12, Supporting Information). Then, Ni K-edge XANES spectra were performed under operando conditions to clarify the transport path of photogenerated electrons (Figure S13, Supporting Information). By using such operando conditions, the possible misinformation caused by the reductive environment created by high-vacuum circumstances when conducting XPS measurement on such a tiny amount of Ni could be avoided. In the XANES spectra, the position of the absorption edge can be reliably used to determine the oxidation state of the investigated element. The more left the absorption edge, the lower the oxidation state (Figure S14, Supporting Information). For a clearer presentation of this position change, Figure 4b displays the derivative operando Ni K-edge XANES spectra. As shown, there is no change in the spectra of 0.5Ni/TiO₂-IM whether the light irradiation is on or not. This means the electron states of NiO_x species do not change during the whole process. For 0.5Ni/TiO₂-MS under the dark condition, in either air atmosphere or glycerol it shows the same position of the Ni K-edge, while ≈0.5 eV shift to the lower energy is observed under light conditions. Once the light irradiation stops, the Ni K-edge returns to its original state. This indicates a decrease in the Ni oxidation state, which ought to result from the acceptance of the photogenerated electrons from the TiO₂ support. The above result shows that the NiO_x nanoparticles on 0.5Ni/TiO₂-IM cannot either receive or donate electrons under light irradiation, while the Ni single atoms can serve as electron acceptors. This is rather understandable because for 0.5Ni/TiO₂-IM, as a part of the Ni²⁺ ions is oxidized to Ni³⁺, some Ni²⁺ ions diffuse to the surface to maintain the charge balance, thus leaving holes inside of NiO_x and making it a p-type semiconductor.^[33] Since TiO₂ is a typical n-type semiconductor, a p–n junction can be formed on the interface between NiO_x and TiO₂. Electrons cannot pass through this junction from TiO₂ to NiO_x due to their band alignment (Figure S15, Supporting Information), so NiO_x cannot act as an electron acceptor.^[34] Furthermore,

when using UV light to excite NiO_x-loaded TiO₂, little light can be harvested by NiO_x due to the large light absorption coefficient of TiO₂ in the UV region and the small amount of NiO_x loaded.^[35] Therefore there is no Ni K-edge shift observed. On the contrary, Ni single atoms form energy levels other than a band. DFT simulations have revealed the special electronic structures when loading Ni single atoms on anatase TiO₂. Such new energy levels are composed of vacant levels formed near the conduction band minimum of TiO₂.^[20] The photogenerated electrons in the TiO₂ conduction band can be transferred to the vacant energy levels in Ni single atoms, which are further transferred to adsorbed O₂.^[36] The chemically adsorbed O₂ molecules on Ni single atoms indicated by O₂-TPD observation can then be reduced by the electrons, forming reactive O₂^{•−} to involve in the subsequent reaction as discussed below.

Electron spin resonance (ESR) spectroscopy was then used to detect the generated ROS (¹O₂, O₂^{•−} and •OH) over different catalysts. Two trapping agents, 2,2,6,6-tetramethylpiperidine (TEMP) and 5,5-dimethyl-1-pyrroline-N-oxide (DMPO) were used for ¹O₂, •OH and O₂^{•−} detection. As shown in Figure 4c, weak 1:1:1 triplet signals are observed under light irradiation over both 0.5Ni/TiO₂-IM and 0.5Ni/TiO₂-MS, which could be identified as 2,2,6,6-tetramethylpiperidine-N-oxyl (TEMPO), suggesting a small amount generation of ¹O₂. In the presence of DMPO in methanol, no obvious signal could be detected over 0.5Ni/TiO₂-IM, while a strong signal associated with DMPO–OOH is observed on 0.5Ni/TiO₂-MS, confirming that a large amount of O₂^{•−} is generated (Figure 4d). In the presence of DMPO in water, a strong 1:2:2:1 quartet signal observed over 0.5Ni/TiO₂-MS under light irradiation suggests the facile generation of •OH (Figure 4e). In conclusion, the facilitated separation and transfer processes of charge carriers, together with the facile oxygen adsorption over single Ni atoms lead to the high-efficiency O₂^{•−} generation, accompanied by •OH radicals due to the reaction between photogenerated holes and water.

Given that several reactive species, including photogenerated holes (h⁺), superoxide (O₂^{•−}), hydroxyl radicals (•OH), and singlet oxygen (¹O₂), could be involved in the glycerol oxidation process, identifying the function of each reactive species is crucial. To this end, we selected triethanolamine (TEOA), superoxide dismutase (SOD), isopropyl alcohol (IPA), and carotene as the scavengers for h⁺, O₂^{•−}, •OH, and ¹O₂, respectively. As shown in Figure 4f, TEOA, SOD, and IPA are found to effectively inhibit glycolaldehyde generation, whereas carotene turns out of little effect on the oxidation rate. Considering the generation of •OH relies on photogenerated holes, the formation of glycolaldehyde should be completed by the cooperative work of superoxide radicals (O₂^{•−}) and hydroxyl radicals (•OH). For the sample prepared by the impregnation method, only TEOA relatively decreases its conversion rate (Figure 4g), thus the unselective oxidation of glycerol over 0.5Ni/TiO₂-IM should be attributed to the photogenerated holes. On the other hand, a similar ¹O₂ species amount exists on both samples (Figure 4c) while it does not have a significant effect on the reaction rate. All these results highlight the importance of the cooperation between superoxide radicals and hydroxyl radicals during glycerol selective C–C cleavage reaction, which can only be enhanced by Ni single atoms for the selective production of glycolaldehyde.



Scheme 1. Proposed reaction mechanism of glycerol oxidation on Ni single atom decorated TiO_2 .

Based on the above results, a tentative mechanism of photocatalytic selective C–C cleavage of glycerol is proposed (Scheme 1). Under light irradiation, electrons are excited to the conduction band while holes are left on the valence band of the TiO_2 photocatalyst. The next crucial step is that electrons transfer to Ni single atoms (as evidenced by operando XANES). The electron-rich Ni single atoms then transfer the electrons to the adsorbed O_2 , forming the reactive $\text{O}_2^{\cdot-}$ radicals, as proved by O_2 -TPD and ESR experiments. The decreased oxygen adsorption energy of single Ni atoms makes $\text{O}_2^{\cdot-}$ radicals desorb more easily from generation sites. Compared with other ROS, the relatively long survival time of $\text{O}_2^{\cdot-}$ radicals enables them to move long distances in water, thus the oxidation reaction can take place beyond the surface of the photocatalyst.^[37] In parallel, the holes transfer to water to generate $\cdot\text{OH}$ radicals. The formed $\cdot\text{OH}$ radicals next activate glycerol (1) to the corresponding carbon-centered radicals (A), accordingly $\cdot\text{OH}$ radicals return to H_2O . The radicals formed by the above reduction and oxidation reactions couple to form (B), following cleavage of C–C, forming glycolaldehyde (2) and other by-products (3). Based on the adsorption energy reported (Table S5, Supporting Information), the formed glycolaldehyde would diffuse into the solution due to the small adsorption energy with TiO_2 , thus avoiding the overoxidation by $\cdot\text{OH}$ on the surface of the photocatalyst, which has a strong oxidizing ability but a short lifetime.^[37] As dihydroxyacetone could not serve as an intermediate to generate glycolaldehyde, while glyceraldehyde can work (without yielding formic acid, shown in Figure S3, Supporting Information), the detected glyceraldehyde during the reaction indicates the possible co-existence of a route to generate glycolaldehyde via glyceraldehyde, but the simultaneous formation of formic acid suggests this is not the major path (Figure 1c). Thus, it could be concluded that the glycolaldehyde is mainly generated by the direct cleavage of glycerol, with the involvement of glyceraldehyde oxidation as a minor route (shown in Scheme 1). In summary, the selectivity of the desired glycolaldehyde product is tuned through the Ni single atoms loaded, where the formation of $\text{O}_2^{\cdot-}$ radicals is the key, which is promoted through efficient charge transfer and O_2 adsorption.

3. Conclusion

We have presented an effective strategy for the highly selective C–C cleavage of biowaste glycerol to produce valuable product glycolaldehyde under ambient conditions driven by light irradiation. Atomically dispersed Ni species, anchored by the novel molten-salt method, present distinctively enhanced performance compared with nickel oxide nanoparticles loaded by the impregnation method. Unlike little catalysis observed on $\text{NiO}_x/\text{TiO}_2$, the optimized single atom photocatalyst $0.5\text{Ni}/\text{TiO}_2\text{-MS}$ results in a two-fold increase in glycolaldehyde evolution rate ($1058 \mu\text{mol g}^{-1} \text{h}^{-1}$) and more importantly a *c.a.* twofold enhancement in selectivity (60.1%) compared with $\text{NiO}_x/\text{TiO}_2$, leading to a turnover number of fifty moles of glycolaldehyde per mole of Ni single atoms. Recycling tests indicate the excellent stability of the nickel species decorated catalysts. Through operando XANES, the facile electron flow from TiO_2 to Ni single atoms under light illumination has been clearly observed, overshadowing NiO_x nanoparticles which cannot either receive or donate electrons. Based on structural analysis and spectroscopic measurements, the superior activity of the catalyst toward selective C–C cleavage of glycerol under ambient conditions can be ascribed to the weakly chemical adsorption of oxygen and effective electron transfer over Ni single atoms, thus efficient generation of superoxide radicals that would shift selectivity to glycolaldehyde. Such properties provide insights into heterogeneous single-atom photocatalysis and could be generally applied as design principles for photocatalytic organic synthesis with improved activity and controlled selectivity.

Supporting Information

Supporting Information is available from the Wiley Online Library or from the author.

Acknowledgements

L.X. and J.T. are thankful for UK EPSRC (EP/R513143/1 and EP/S018204/2), Leverhulme Trust (RPG-2017-122), Royal Society Newton Advanced Fellowship grant (NAF\R1\191163), Royal Society Leverhulme Trust Senior Research Fellowship (SRF\R1\21000153). H.Q., S.Z., L.Z., X.L., and A.W. are thankful for financial support from the National Natural Science Foundation of China (22132006, 21878289, and 22172159) and CAS Project for Young Scientists in Basic Research (YSBR-022).

Conflict of Interest

The authors declare no conflict of interest.

Data Availability Statement

The data that support the findings of this study are available from the corresponding author upon reasonable request.

Keywords

biomass derivatives, glycerol, glycolaldehyde, selective oxidation, single-atom photocatalysts

Received: October 19, 2022
Revised: January 23, 2023
Published online: March 12, 2023

- [1] a) C.-H. (C.) Zhou, J. N. Beltrami, Y.-X. Fan, G. Q. (M.) Lu, *Chem. Soc. Rev.* **2008**, *37*, 527; b) K. E. Sanwald, T. F. Berto, W. Eisenreich, O. Y. Gutiérrez, J. A. Lercher, *J. Catal.* **2016**, *344*, 806; c) Y. Wan, J.-M. Lee, *ACS Catal.* **2021**, *11*, 2524.
- [2] S.-H. Shi, Y. Liang, N. Jiao, *Chem. Rev.* **2021**, *121*, 485.
- [3] C. A. G. Quispe, C. J. R. Coronado, J. A. Carvalho, Jr, *Renewable Sustainable Energy Rev.* **2013**, *27*, 475.
- [4] J. J. Bozell, G. R. Petersen, *Green Chem.* **2010**, *12*, 539.
- [5] a) Z. Wang, L. Wang, Y. Jiang, M. Hunger, J. Huang, *ACS Catal.* **2014**, *4*, 1144; b) M. H. Haider, N. F. Dummer, D. Zhang, P. Miedziak, T. E. Davies, S. H. Taylor, D. J. Willock, D. W. Knight, D. Chadwick, G. J. Hutchings, *J. Catal.* **2012**, *286*, 206.
- [6] a) S. Feng, J. Yi, H. Miura, N. Nakatani, M. Hada, T. Shishido, *ACS Catal.* **2020**, *10*, 6071; b) P. M. Walgode, R. P. V. Faria, A. E. Rodrigues, *Catal. Rev.* **2021**, *63*, 422.
- [7] a) C. D. Evans, M. Douthwaite, J. H. Carter, S. Pattison, S. A. Kondrat, D. Bethell, D. W. Knight, S. H. Taylor, G. J. Hutchings, *J. Chem. Phys.* **2020**, *152*, 134705; b) M. Douthwaite, N. Powell, A. Taylor, G. Ford, J. M. López, B. Solsona, N. Yang, O. Sanahuja-Parejo, Q. He, D. J. Morgan, T. Garcia, S. H. Taylor, *ChemCatChem* **2020**, *12*, 3097.
- [8] S. Bagheri, N. M. Julkapli, W. A. Yehye, *Renewable Sustainable Energy Rev.* **2015**, *41*, 113.
- [9] a) T. Gabrysch, B. Peng, S. Bunea, G. Dyker, M. Muhler, *ChemCatChem* **2018**, *10*, 1344; b) Y.-S. Feng, C. Liu, Y.-M. Kang, X.-M. Zhou, L.-L. Liu, J. Deng, H.-J. Xu, Y. Fu, *Chem. Eng. J.* **2015**, *281*, 96; c) C. Wang, H. Jiang, C. Chen, R. Chen, W. Xing, *Chem. Eng. J.* **2015**, *264*, 344.
- [10] F. Wu, H. Jiang, X. Zhu, R. Lu, L. Shi, F. Lu, *ChemSusChem* **2021**, *14*, 569.
- [11] F. Porta, L. Prati, *J. Catal.* **2004**, *224*, 397.
- [12] H. Yan, Q. Shen, Y. Sun, S. Zhao, R. Lu, M. Gong, Y. Liu, X. Zhou, X. Jin, X. Feng, X. Chen, D. Chen, C. Yang, *ACS Catal.* **2021**, *11*, 6371.
- [13] L. Xiong, J. Tang, *Adv. Energy Mater.* **2021**, *11*, 2003216.
- [14] a) Y. Zhang, N. Zhang, Z.-R. Tang, Y.-J. Xu, *Chem. Sci.* **2013**, *4*, 1820; b) R. Chong, J. Li, X. Zhou, Y. Ma, J. Yang, L. Huang, H. Han, F. Zhang, C. Li, *Chem. Commun.* **2014**, *50*, 165.
- [15] X. Jin, C. Li, C. Xu, D. Guan, A. Cheruvathur, Y. Wang, J. Xu, D. Wei, H. Xiang, J. W. (H.) Niemantsverdriet, Y. Li, Q. Guo, Z. Ma, R. Su, X. Yang, *J. Catal.* **2017**, *354*, 37.
- [16] C. Li, X. Wang, A. Cheruvathur, Y. Shen, H. Xiang, Y. Li, J. W. (H.) Niemantsverdriet, R. Su, *J. Catal.* **2018**, *365*, 313.
- [17] a) V. Augugliaro, H. A. H. El Nazer, V. Loddo, A. Mele, G. Palmisano, L. Palmisano, S. Yurdakal, *Catal. Today* **2010**, *151*, 21; b) S. Yurdakal, G. Palmisano, V. Loddo, V. Augugliaro, L. Palmisano, *J. Am. Chem. Soc.* **2008**, *130*, 1568.
- [18] Y. Nosaka, A. Y. Nosaka, *Chem. Rev.* **2017**, *117*, 11302.
- [19] C. Gao, J. Low, R. Long, T. Kong, J. Zhu, Y. Xiong, *Chem. Rev.* **2020**, *120*, 12175.
- [20] A. Iwaszuk, M. Nolan, Q. Jin, M. Fujishima, H. Tada, *J. Phys. Chem. C* **2013**, *117*, 2709.
- [21] Z.-H. Xue, D. Luan, H. Zhang, X. W. Lou, *Joule* **2022**, *6*, 92.
- [22] M. Xiao, L. Zhang, B. Luo, M. Lyu, Z. Wang, H. Huang, S. Wang, A. Du, L. Wang, *Angew. Chem., Int. Ed.* **2020**, *59*, 7230.
- [23] S. Shen, J. Chen, M. Wang, X. Sheng, X. Chen, X. Feng, S. S. Mao, *Prog. Mater. Sci.* **2018**, *98*, 299.
- [24] C. Zhao, Y. Wang, Z. Li, W. Chen, Q. Xu, D. He, D. Xi, Q. Zhang, T. Yuan, Y. Qu, J. Yang, F. Zhou, Z. Yang, X. Wang, J. Wang, J. Luo, Y. Li, H. Duan, Y. Wu, Y. Li, *Joule* **2019**, *3*, 584.
- [25] C. A. Tolman, W. M. Riggs, W. J. Linn, C. M. King, R. C. Wendt, *Inorg. Chem.* **1973**, *12*, 2770.
- [26] H. W. Nesbitt, D. Legrand, G. M. Bancroft, *Phys. Chem. Miner.* **2000**, *27*, 357.
- [27] Y. S. Chen, J. F. Kang, B. Chen, B. Gao, L. F. Liu, X. Y. Liu, Y. Y. Wang, L. Wu, H. Y. Yu, J. Y. Wang, Q. Chen, E. G. Wang, *J. Phys. D: Appl. Phys.* **2012**, *45*, 065303.
- [28] Z. Wang, X. Mao, P. Chen, M. Xiao, S. A. Monny, S. Wang, M. Konarova, A. Du, L. Wang, *Angew. Chem., Int. Ed.* **2019**, *58*, 1030.
- [29] P. Doggali, Y. Teraoka, P. Mungse, I. K. Shah, S. Rayalu, N. Labhsetwar, *J. Mol. Catal. A: Chem.* **2012**, *358*, 23.
- [30] J. M. McKay, V. E. Henrich, *J. Vac. Sci. Technol., A* **1987**, *5*, 722.
- [31] H. Gu, X. Liu, X. Liu, C. Ling, K. Wei, G. Zhan, Y. Guo, L. Zhang, *Nat. Commun.* **2021**, *12*, 5422.
- [32] a) W. Gu, X. Wang, J. Wen, S. Cao, L. Jiao, Y. Wu, X. Wei, L. Zheng, L. Hu, L. Zhang, C. Zhu, *Anal. Chem.* **2021**, *93*, 8663; b) M. Setvín, U. Aschauer, P. Scheiber, Y.-F. Li, W. Hou, M. Schmid, A. Selloni, U. Diebold, *Science* **2013**, *341*, 988.
- [33] D. Irwin Michael, D. B. Buchholz, W. Hains Alexander, P. H. Chang Robert, J. Marks Tobin, *Proc. Natl. Acad. Sci. USA* **2008**, *105*, 2783.
- [34] M. Wang, Y. Hu, J. Han, R. Guo, H. Xiong, Y. Yin, *J. Mater. Chem. A* **2015**, *3*, 20727.
- [35] C.-J. Chen, C.-H. Liao, K.-C. Hsu, Y.-T. Wu, J. C. S. Wu, *Catal. Commun.* **2011**, *12*, 1307.
- [36] Q. Jin, T. Ikeda, M. Fujishima, H. Tada, *Chem. Commun.* **2011**, *47*, 8814.
- [37] D. Wang, L. Zhao, H. Ma, H. Zhang, L.-H. Guo, *Environ. Sci. Technol.* **2017**, *51*, 10137.